Human species D adenovirus hexon capsid protein mediates cell entry through a direct interaction with CD46

B. David Persson[a,b,1], Lijo John[a,b,1], Karim Rafie[b,c,d], Michael Strebl[e], Lars Frängsmyr[a,b], Monika Z. Ballmann[f], Katja Mindler[e], Menzo Havenga[f], Angelique Lemckert[f], Thilo Stehle[e], Lars-Anders Carlson[b,c,d], and Niklas Arnberg[a,b,2]

[a]Department of Clinical Microbiology, Division of Virology, Umeå University, SE-90185 Umeå, Sweden; [b]Laboratory for Molecular Infection Medicine Sweden, Umeå University, SE-90185 Umeå, Sweden; [c]Wallenberg Centre for Molecular Medicine, Umeå University, SE-90187 Umeå, Sweden; [d]Department of Medical Biochemistry, Umeå University, SE-90187 Umeå, Sweden; [e]Interfaculty Institute of Biochemistry, The University of Tübingen, D-72076 Tübingen, Germany; and [f]Batavia Biosciences, 2333 CL Leiden, The Netherlands

Edited by Thomas Shenk, Princeton University, Princeton, NJ, and approved November 30, 2020 (received for review October 3, 2020)

Human adenovirus species D (HAdV-D) types are currently being explored as vaccine vectors for coronavirus disease 2019 (COVID-19) and other severe infectious diseases. The efficacy of such vector-based vaccines depends on functional interactions with receptors on host cells. Adenoviruses of different species are assumed to enter host cells mainly by interactions between the knob domain of the protruding fiber capsid protein and cellular receptors. Using a cell-based receptor-screening assay, we identified CD46 as a receptor for HAdV-D56. The function of CD46 was validated in infection experiments using cells lacking and overexpressing CD46, and by competition infection experiments using soluble CD46. Remarkably, unlike HAdV-B types that engage CD46 through interactions with the knob domain of the fiber protein, HAdV-D types infect host cells through a direct interaction between CD46 and the hexon protein. Soluble hexon proteins (but not fiber knob) inhibited HAdV-D56 infection, and surface plasmon analyses demonstrated that CD46 binds to HAdV-D hexon (but not fiber knob) proteins. Cryoelectron microscopy analysis of the HAdV-D56 virion–CD46 complex confirmed the interaction and showed that CD46 binds to the central cavity of hexon trimers. Finally, soluble CD46 inhibited infection by 16 out of 17 investigated HAdV-D types, suggesting that CD46 is an important receptor for a large group of adenoviruses. In conclusion, this study identifies a noncanonical entry mechanism used by human adenoviruses, which adds to the knowledge of adenovirus biology and can also be useful for development of adenovirus-based vaccine vectors.

adenovirus | hexon | CD46 | receptor | vaccine

Wild-type human adenoviruses (HAdVs) are associated with a broad range of more or less severe clinical manifestations in respiratory, lymphoid, gastrointestinal, and ocular tissues (1). To date, more than 100 HAdV types have been identified, and classified into seven species, A through G (2). HAdV species D comprises two-thirds of all known types and exhibits features that make these types attractive as vaccine vectors (3–7). Thus, HAdV-D types are currently being explored as vaccine vectors for prevention against infections caused by, for example, severe acute respiratory syndrome coronavirus 2 (8–10), HIV (11), respiratory syncytial virus (12), Ebola virus (13), and Zika virus (14). The presence and engagement of functional receptors on relevant host cells are features that are crucial for the efficacy of adenovirus-based vector vaccines, and knowledge about such interactions is of importance since this allows detargeting of vectors to native receptors present on less relevant cells but also opens up for retargeting of vectors to relevant host cells.

HAdV-A and C through G types enter host cells through interactions with the Coxsackievirus and adenovirus receptor (CAR) (15–17), and HAdV-B types interact with CD46 and/or desmoglein-2 (DSG2) (18–21). HAdV-D37 and a few other HAdV-D types interact with sialic acid-containing glycans (22, 23). These interactions are all mediated by the knob domain of the fiber capsid protein. HAdV-D37 and several other distinct HAdV-D types have also been reported to use CD46 as a cellular receptor (3, 5, 24–31), a protein that is expressed on all human nucleated cells including dendritic cells (3). Remarkably, whereas the interactions between HAdV-B types and CD46 are well-characterized and clearly depend on the fiber protein (18–20, 32), little is known about the mechanism whereby HAdV-D types engage CD46. One study suggests that HAdV-D37 interacts with CD46 through the fiber knob domain (27), but this interaction has not been functionally or structurally validated. In this study, we demonstrate that HAdV-D56 and D26 engage CD46 through a nonconventional interaction involving the hexon instead of the fiber, and that 16 out of 17 randomly selected HAdV-D types use CD46 as a cellular receptor.

Results

Identification and Validation of CD46 as a Cellular Receptor for HAdV-D56. To identify CD46 as a cellular receptor for HAdV-D56, we

Significance

The adenovirus capsid protein is built by three main capsomers: hexon, fiber, and penton base. Entry is mediated by fiber proteins anchoring the virus to host cell receptors and is followed by penton base proteins engaging coreceptors, resulting in entry. Here, we demonstrate that human adenovirus species D types, which constitute two-thirds of all human adenoviruses, enter host cells through a direct interaction between the hexon protein and CD46. This study provides insights into the entry mechanisms used by human adenoviruses. As these viruses are also used as vaccine vectors for prevention of other infectious diseases, the results provided will also be useful for further development of human adenovirus species D types as vaccine vectors.

Author contributions: B.D.P., L.J., K.R., M.S., L.F., K.M., T.S., L.-A.C., and N.A. designed research; B.D.P., L.J., K.R., M.S., L.F., and K.M. performed research; M.Z.B., M.H., and A.L. contributed new reagents/analytic tools; B.D.P., L.J., K.R., M.S., L.F., K.M., T.S., L.-A.C., and N.A. analyzed data; and B.D.P. and N.A. wrote the paper.

Competing interest statement: M.Z.B., M.H., and A.L. are employees of Batavia Biosciences.

This article is a PNAS Direct Submission.

[1]Present address: National Veterinary Institute, SE-75189 Uppsala, Sweden.

[2]To whom correspondence may be addressed. Email: niklas.arnberg@umu.se.

This article contains supporting information online at https://www.pnas.org/lookup/suppl/doi:10.1073/pnas.2020732118/-/DCSupplemental.

Published December 31, 2020.

transduced Chinese hamster ovary (CHO) cells that either overexpress or lack known human adenovirus receptors (33) with an enhanced green fluorescent protein (eGFP)-expressing HAdV-D56 vector (34). Data obtained demonstrated that HAdV-D56 transduced CD46- (isoform C2) overexpressing CHO cells efficiently (Fig. 1*A* and *SI Appendix*, *Results* and Fig. S1). In contrast, cells overexpressing the Coxsackievirus and adenovirus receptor (CHO-CAR), or lacking sialic acid (Lec2), heparan sulfate (CHO-677), or glycosaminoglycans (CHO-618), and their respective control cells CHO-MOCK, Pro-5, and CHO-K1 (control for both 677 and 618 cells) were transduced weakly or not at all. As expected, a GFP-expressing, HAdV-C5 reference vector only transduced cells expressing the HAdV-C5 receptor CAR (33). Next, we observed superior binding to CHO-CD46 cells with both ^{35}S-labeled HAdV-D56 and B35 (but not C5) virions as compared with control CHO-K1 cells (Fig. 1*B*). GFP-encoding HAdV-D56 and HAdV-C5/F35 vectors (the latter is based on HAdV-C5 but is equipped with a fiber from HAdV-B35) transduced CD46-deficient human HAP1 cells less efficiently as compared with corresponding, CD46-expressing control cells (Fig. 1*C*), whereas the CAR-binding HAdV-C5 vector (with C5 fiber) transduced both cells equally well. Furthermore, soluble CD46 (but not soluble CAR) inhibited transduction of CHO-CD46 cells by HAdV-D56 and C5/F35 vectors in a dose-dependent manner (Fig. 1*D*). We noted that soluble CD46 inhibited transduction of HAdV-C5/F35 completely and HAdV-D56 incompletely, suggesting that CD46 is not the only receptor used by HAdV-D56 on these cells.

HAdV-D56 Hexon Protein Engages CD46 but Not the Fiber. It is generally accepted that adenoviruses bind to host cell receptors foremost through interactions mediated by the knob domain of the fiber protein (33), including CD46-binding HAdV-B types. A number of HAdV-D types also engage CD46, but the mechanism of interaction is unclear (5, 6, 24–27, 31). To determine whether HAdV-D56 also interacts with the fiber knob, we first investigated if soluble fiber knobs from HAdV-C5 (binds CAR), B7 (binds CD46 with low affinity), B35 (binds CD46 with high affinity), and D56 interfered with transduction of CD46-expressing CHO cells by GFP-expressing HAdV-D56 vectors. Surprisingly, only HAdV-B35 fiber knobs reduced HAdV-D56 transduction, and only to about 75%, which was less efficient than the close to 100% inhibition observed with HAdV-5/F35 transduction with the same knob (*SI Appendix*, Fig. S2*A*). Flow cytometry experiments showed that fiber knobs of HAdV-D56 and B7 did not bind better to CHO-CD46 cells than to CHO-K1 cells but fiber knobs of HAdV-B35 did bind better (*SI Appendix*, Fig. S2*B*), indicating that HAdV-D56 may bind to CD46 through a fiber-independent mechanism. In an attempt to address this question, we performed surface plasmon resonance (SPR) analyses of virion and knob binding to immobilized CD46. As expected, both HAdV-B35 fiber knobs and virions bound efficiently to CD46 (Fig. 2 *A* and *B*); however, whereas HAdV-D56 fiber knobs failed to bind CD46, virions did bind (Fig. 2 *C* and *D*). HAdV-B7 virions and knobs did not bind to CD46 (*SI Appendix*, Fig. S2 *C* and *D*), which contradicts a previous study reporting that HAdV-B7 binds to CD46 via fiber knobs through a low affinity–high avidity interaction (35); however, in that study, CD46 was immobilized at a much higher level than in our study, which may explain this discrepancy. As expected, neither HAdV-C5 virions nor fiber knobs bound to CD46 (*SI Appendix*, Fig. S2 *E* and *F*). Fiber knob homology alignment demonstrated that the HAdV-D56 fiber knob lacks important CD46-interacting amino acids (32, 36–38) (*SI Appendix*, Fig. S2*G*) and X-ray crystallography of HAdV-56 fiber knobs followed by docking analyses (*SI Appendix*, Fig. S2*H*) demonstrated that the known CD46-interacting loops (DG, HI, and IJ) were disordered in HAdV-D56 as compared with HAdV-B11, which binds with high affinity to CD46 (39). These observations led us to hypothesize that HAdV-D56 interacts with CD46 through a noncanonical (fiber-independent) interaction. To investigate if HAdV-D56 bound to CD46 via the hexon protein, we analyzed this interaction by SPR. Surprisingly, soluble HAdV-D56 as well as D26 hexons bound to immobilized CD46 (Fig. 2 *E* and *F*), with similar, intermediate affinities (*SI Appendix*, Table S1). A role of the hexon in CD46-mediated entry was also suggested from infection competition experiments showing that HAdV-D56 and D26 hexons (but not the HAdV-D56 fiber knob) inhibited HAdV-D56 infection (Fig. 2*G*).

Structural Analysis of HAdV-D56 Interaction with CD46. To finally validate this noncanonical interaction, we performed cryoelectron microscopy (cryo-EM) analysis to solve the structure of HAdV-56 virions in the absence and presence of CD46, to 4.8 and 5.1 Å, respectively. Comparing the two maps, HAdV-D56–CD46 (Fig. 3*B*) contains additional electron density not present in the HAdV-D56 map (Fig. 3*A*). This additional density is located above the hexon towers at both peripentonal and nonperipentonal hexons. The CD46 density is weaker than that of the capsid, indicating substoichiometric engagement of CD46 by the capsid or possibly a heterogeneity in the conformation of the binding. As a further visualization of the additional densities, we calculated a difference map between the HAdV-D56–CD46 and HAdV-D56 structures. The difference map shows the additional densities at the central cavities at the top of the hexons (compare Fig. 3*C* with Fig. 3*D*, and Fig. 3*E* with Fig. 3*F*), similar to the interactions observed between the HAdV-C5 hexon and coagulation factor X (40). The difference map also indicates that the α-helical bundle formed by four copies of pIX shifts slightly upon CD46 binding (*SI Appendix*, Fig. S3 *A* and *B*). We cannot exclude that CD46 also interacts with pIX, but hypothesize that these positional shifts in pIX densities result from a slight conformational change in the hexon during interaction with CD46. The density of the pentons (containing penton base and fiber proteins) is poorly resolved in the cryo-EM structures of both HAdV-D56 and HAdV-D56–CD46, probably because these proteins are more flexible with respect to the icosahedral capsid than other capsid proteins.

Soluble CD46 Prevents Infection of A549 Cells by a Majority of HAdV-D Types. Finally, to further investigate the role of CD46 during infection of human cells by HAdV-D types, we quantified infection of human A549 cells by 17 selected HAdV types in the presence of soluble CD46. Strikingly, with the exception of HAdV-D37—an ocular serotype that binds to sialic acid-containing glycans resembling those present in GD1a gangliosides (23)—and CAR-binding HAdV-C5, infection of all investigated types was inhibited by up to 90%, and at least 50% (Fig. 4). With a few exceptions, the 17 types represent most arms in a phylogenetic tree built by all known HAdV-D hexon proteins (*SI Appendix*, Fig. S4), implying that a majority of all HAdV-D types may use CD46 as a preferred receptor.

Discussion

In summary, we conclude that HAdV-D56 engages CD46 as a receptor for cell entry through direct interactions with the hexon protein. This is a noncanonical mechanism in relation to what is known about adenovirus entry in general, where receptors such as CAR, CD46, DSG2, and sialic acid-containing glycans are engaged by means of the fiber protein (33). As CAR and DSG2 are both cell-adhesion molecules that are not abundant on, for example, antigen-presenting cells (41, 42), it is reasonable to expect that vaccine vectors based on adenoviruses will transduce antigen-presenting cells more efficiently if they engage other receptors, which are present on these cells. CD46 is expressed on all human nucleated cells, including antigen-presenting cells, suggesting that CD46-engaging (e.g., HAdV-D) types transduce these cells more efficiently than CAR-engaging (e.g., HAdV-B)

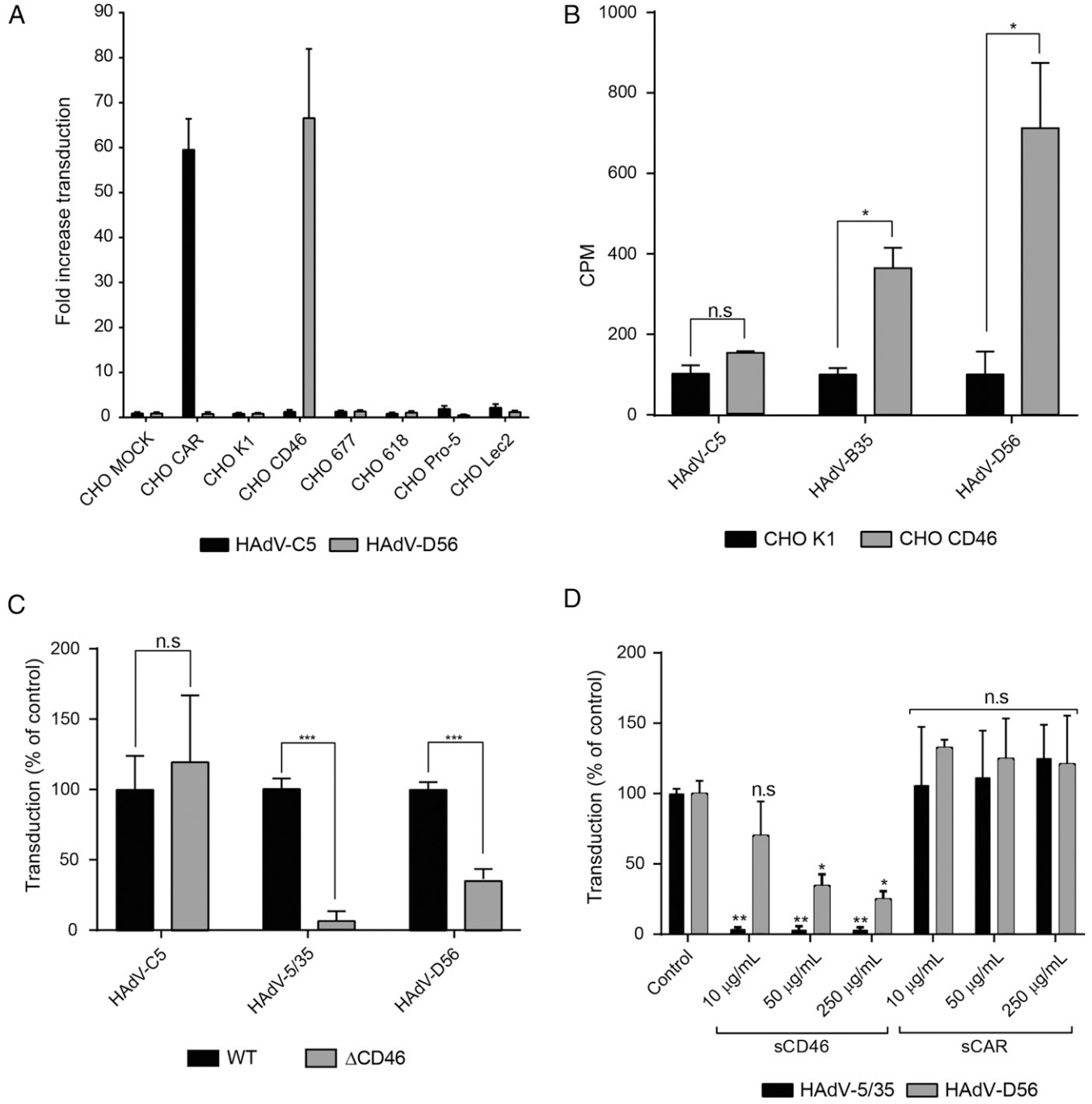

Fig. 1. Identification and validation of CD46 as a cellular receptor for HAdV-D56. (*A*) Transduction by HAdV-D56–GFP in CHO cells stably expressing or lacking known human adenovirus receptors. The levels of transduction are presented as fold change relative to the CHO-MOCK. (*B*) Attachment of wild-type ^{35}S-labeled HAdV-D56, HAdV-C5, and HAdV-B35 virions to CHO cells expressing or lacking human CD46. (*C*) Transduction of GFP-encoding HAdV-C5, HAdV-D56, and HAdV-5/35 vectors in HAP1 cells expressing or lacking CD46. (*D*) Transduction of GFP-encoding HAdV-D56 and HAdV-5/35 vectors in CHO-CD46 cells in the presence of increasing amounts of soluble CD46 or CAR. All data are presented as mean ± SEM from three independent experiments in duplicates, where $*P \leq 0.05$, $**P \leq 0.01$, and $***P \leq 0.001$; n.s, not significant.

types. Moreover, it was recently shown that preexisting, neutralizing antibodies against a COVID-19 vaccine based on HAdV-C5 affected the efficiency of the vaccine candidate (43). Thus, an advantage of using CD46-targeting HAdV-D types is that the seroprevalence is in general lower against many of these types (44), which would allow such vectors to be efficient either as single-dose vectors or in combination with vectors based on other HAdV-D types. HAdV-D37 was the only type not inhibited by soluble CD46 in our study, but this does not exclude that HAdV-37 also engages CD46 through the hexon protein. We have previously shown that this serotype uses sialic acid-containing glycans as receptors by engaging the fiber protein (23). However, this serotype has also been proposed to use CD46 as a receptor (27, 31). Another related serotype—HAdV-D26, which is currently used as a vector for vaccination against COVID-19—also binds sialic acid via the fiber protein (22). In our study, we show

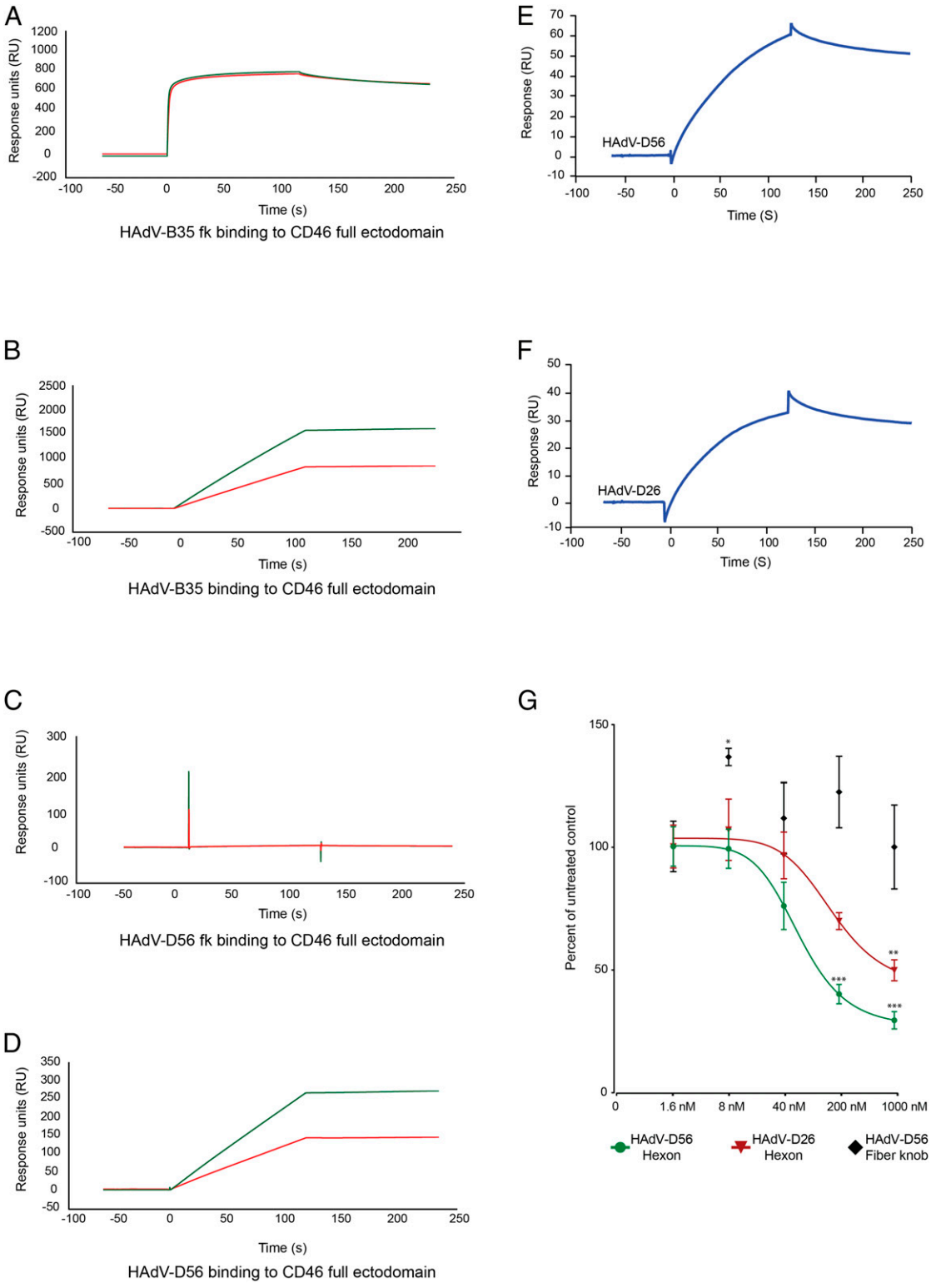

Fig. 2. HAdV-D56 hexon protein engages CD46 but not the fiber. (*A–F*) SPR analyses of the HAdV-B35 fiber knob (*A*), HAdV-B35 virion (*B*), HAdV-D56 fiber knob (*C*), HAdV-D56 virion (*D*), HAdV-D56 hexon (*E*), and HAdV-D26 hexon (*F*) binding to immobilized CD46. (*G*) HAdV-D56 transduction of A549 cells in the presence of increasing concentrations of soluble hexon (HAdV-D56 or D26) or fiber knob (HAdV-D56). All data are presented as mean ± SEM from three independent experiments in duplicates, where $*P \leq 0.05$, $**P \leq 0.01$, and $***P \leq 0.001$.

that HAdV-D26 also interacts with CD46 via the hexon protein. Altogether, there is emerging evidence suggesting that receptor interactions by HAdV-D types are complex and that some types enter host cells by at least two distinct mechanisms, including fiber–sialic acid interactions and hexon–CD46 interactions. Whereas the sialic acid-dependent interaction has been investigated in detail and clearly relies on the fiber knob (23, 45), the mechanism of the CD46-dependent interaction has only been addressed in a few

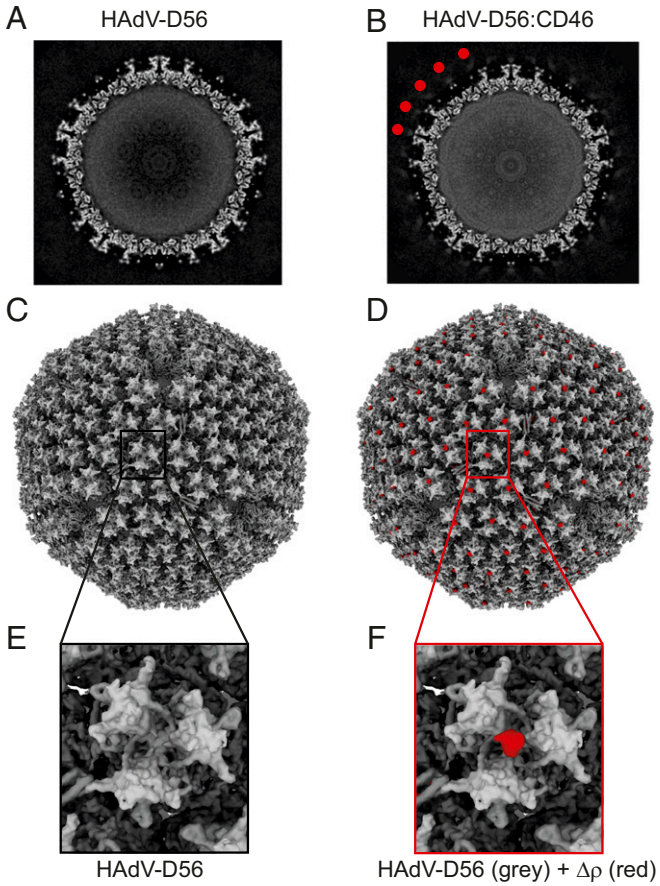

Fig. 3. Structural analysis of HAdV-D56 interaction with CD46. (*A*) Computational slice through the HAdV-D56 volume. (*B*) Computational slice through the HAdV-D56–CD46 volume. Delocalized density belonging to CD46 is highlighted by red dots at a few positions. (*C*) Surface representation of the reconstructed HAdV-D56 electron density (gray) at 4.8 Å. (*D*) Surface representation of the reconstructed HAdV-D56 electron density (gray) overlaid with the difference map Δρ (HAdV-D56–CD46 − HAdV-D56) low-pass–filtered to 10 Å showing density belonging to CD46 (red). (*E*) Zoom-in on an HAdV-D56 hexon. (*F*) Zoom-in on an HAdV-D56 hexon overlaid with the difference map Δρ low-pass–filtered to 10 Å showing density belonging to CD46 (red).

studies, and rarely in depth. In most studies (3, 5, 26, 28), HAdV-D–type transduction is investigated using cells or animals that express or lack CD46, or competition studies are performed using soluble CD46 or antibodies blocking CD46. Belousova et al. (25) demonstrated that HAdV-D17 vectors transduced CD46-expressing cells better than control cells, but HAdV-D17 fibers did not inhibit transduction and HAdV-D43 fiber knobs only inhibited HAdV-D17 transduction at very high concentrations. In Lecollinet et al. (30) it was demonstrated that anti-CD46 serum slightly inhibited HAdV-C5 vectors equipped with fibers from HAdV-D8 but not HAdV-C5 vectors with fibers from D32. And, Wu et al. (27) demonstrated that HAdV-C5 vectors equipped with D37 fibers transduced CD46-expressing cells better than control cells and that antibodies against CD46 inhibited this transduction, which is perhaps the best evidence for a functional interaction between CD46 and an HAdV-D type. However, none of these studies provide functional data showing that wild-type HAdV-D types infect target cells by means of direct fiber interactions with CD46 or structural data demonstrating a physical interaction between HAdV-D fibers and CD46. The study by Wu et al. is remarkable in the sense that in our hands, HAdV-D37 was the only type that was not significantly inhibited by soluble CD46, a discrepancy that may potentially be explained by usage of different cell types or usage of a wild-type virus versus a pseudotyped vector, or both combined. It should also be noted that in addition to usage of sialic acid or CD46, some HAdV-D fibers also interact with CAR (16, 46, 47). Remarkably, HAdV-D37 fiber knobs are reported to interact with CAR with relatively high affinity (20 nM) (47) but are suggested not to use CAR as a receptor, in part due to the rigidity of this fiber, which prevents intact virions from interacting with CAR on target cells (48). The relatively high affinity may be related to the function of excess fibers that are produced and secreted from cells infected by many different HAdV types, and may contribute to more efficient transmission of progeny virus as suggested by others (49, 50). Another interaction that regulates the tropism of HAdV-based vectors, for example for vaccination, is hexon interactions with coagulation factors including factor X (40). Among the HAdV-D types investigated by Waddington et al. (40), 4 out of 12 investigated D types (i.e., D13, D37, D46, and D49) engage factor X. The relative function and importance of these interactions and if they interfere with potential CD46 interactions are unclear. Thus, further studies are needed to determine the relative contribution of each mechanism for cell tropism and entry into, for example, antigen-presenting cells by different HAdV-D types, which can contribute to the selection and design of HAdV-D types for development as vaccine vectors.

Materials and Methods

Cells, Viruses, Antibodies, and Recombinant Proteins. Human haploid (HAP1) wild-type and CD46 knockout cells were purchased from Horizon. All HAP1 cells were maintained in Iscove's Modified Dulbecco's Medium (IMDM; Gibco) supplemented with 10% (volume/volume; vol/vol) fetal bovine serum (FBS) (HyClone) and 1× PenStrep (100 μg/mL penicillin and 100 U/mL streptomycin; Gibco). CHO-CAR and CHO-MOCK cells were a generous gift from Jeffrey M. Bergelson, Children's Hospital of Philadelphia, Philadelphia, PA, and CD46-expressing CHO cells (isoforms BC1, BC2, C1, and C2) were a generous gift from John P. Atkinson, Washington University School of Medicine, Saint Louis, MO. The additional CHO cells (K1, CHO Pro5, and CHO Lec2) were purchased from ATCC. All CHO cells were grown as previously described (15, 51). A549 cells were grown in DPH (1× DMEM, PenStrep, 20 mM Hepes, pH 7.4) + 10% FBS. Species D HAdV-D56–eGFP was produced as described (34). HAdV-C5–eGFP and HAdV-5/35–eGFP were purchased from the Vector Development Laboratory. Wild-type adenoviruses (prototype strains) HAdV-D56, HAdV-D26, HAdV-C5, HAdV-B35, and HAdV-B7 were produced in A549 cells with or without ^{35}S labeling and purified on cesium chloride (CsCl) gradients as described previously (52). Monoclonal antibodies directed against CD46 (BD Biosciences) and donkey Alexa Fluor 488-conjugated secondary antibody (Invitrogen) were used in flow cytometry. In competition assays, we used soluble CD46 (Sino Biological), and CD46 SCR1 to 4 and CAR-D1 were produced as previously described (53, 54).

Expression and Purification of Soluble Fiber Knobs. Fiber knob proteins of HAdV-B35, HAdV-C5, HAdV-D37, and HAdV-B7 were expressed in *Escherichia coli* as described previously (17). For the HAdV-D56 fiber knob, residues 167 to 362 of the HAdV-D56 fiber knob were cloned into a pQE-30XA vector containing an N-terminal 6His tag. The construct was expressed in *E. coli* BL21 (DE3) (Stratagene) for ∼5 h at 37 °C after induction with 1 mM isopropyl β-D-1-thiogalactopyranoside. Cells were harvested and the pellet was resuspended in lysis buffer (30 mM Tris·HCl, pH 7.4, 150 mM NaCl, 30 mM imidazole) with additional 1 mM phenylmethanesulfonylfluoride and 1 mM $MgCl_2$. Cells were lysed by sonication and centrifuged at 35,000 × *g* for 45 min at 4 °C. The supernatant was loaded onto a 5-mL HisTrap FF crude column (GE Healthcare) and protein was eluted after washing by applying a linear imidazole gradient ranging from 30 to 500 mM. Fractions were pooled, concentrated, and purified over a HiLoad 16/60 Superdex 200 (GE Life Sciences) with gel-filtration buffer (30 mM Tris·HCl, pH 7.4, 150 mM NaCl). For crystallization, the HAdV-D56 fiber knob was concentrated to 20.8 mg/mL.

Hexon Purification. Ten flasks of A549 cells were infected using HAdV-D56 and HAdV-D26 and after 48 h were harvested by scraping off the cells.

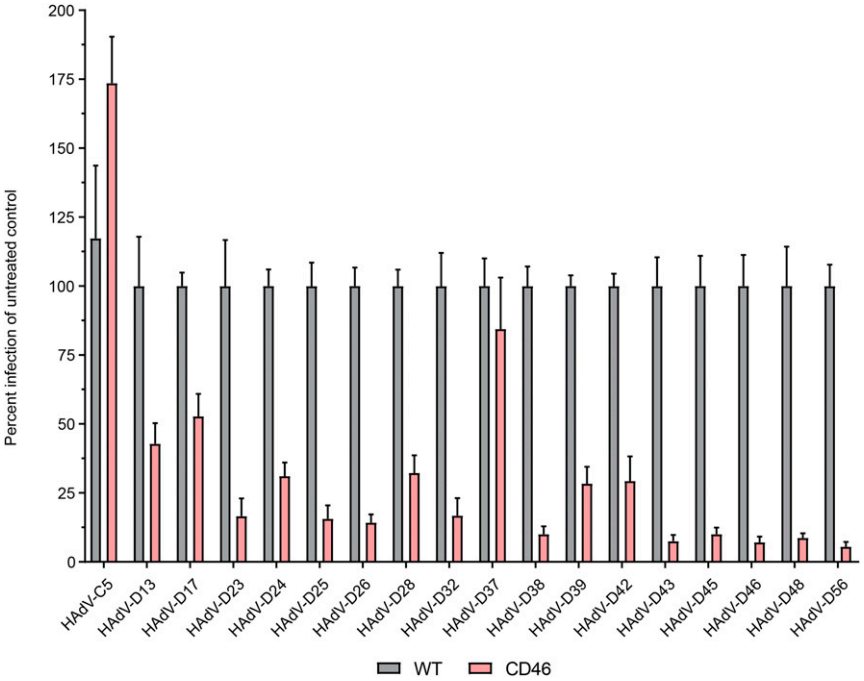

Fig. 4. Soluble CD46 prevents infection of A549 cells by a majority of HAdV-D types. Quantification of infection (staining of hexon production) in A549 cells 44 h after HAdV wild-type infection in the presence or absence of soluble CD46 (50 μg/mL). All data are presented as mean ± SEM from two independent experiments in duplicates. All differences are statistically significant ($P < 0.05$ or better) except for HAdV-C5 and D37.

Cell-containing supernatant was pelleted and the cellular pellet was resuspended in 5 mL of DMEM. Once resuspended, the cells were lysed by three repeating freeze/thaw cycles and then vigorously shaken with Vertrel (Sigma), and cellular debris was pelleted by centrifugation. The clear virus-containing liquid was loaded onto a conventional CsCl gradient to separate intact virus particles from soluble components. After ultracentrifugation, the top phase was collected and concentrated on a 100-kDa cutoff concentrator. At the same time, the DMEM was replaced with the buffer used for size-exclusion chromatography, a buffer containing 20 mM Hepes (pH 7.4), 150 mM NaCl, by topping off the concentrator five times. After concentration, 3 to 4 mL of material was loaded on a Superose 6 column and fractions roughly corresponding to a trimer of hexon were recovered. Purity was assessed by sodium dodecyl sulfate-polyacrylamide gel electrophoresis and the identity of the purified protein was assessed by mass spectrometry. Hexon for HAdV-C5 was purchased from Bio-Rad.

Transduction Experiments. Transductions were carried out on cells grown as monolayers in black 96-well plates. Before all transduction experiments, the cells were washed with plain DMEM, or IMDM, to remove all serum components. Subsequently, the virions were added to the cells and incubated for 60 min. After transduction, the cells were washed with DMEM/IMDM to remove all unbound virions, followed by the addition of cell-culture medium containing 2% FBS, or 5% for HAP1 cells. At 24 h postinfection (hpi), cells were fixed with 4% paraformaldehyde for 15 min and stained with Hoechst 3342 diluted 1:10,000 at room temperature for 10 min. When using wild-type virus instead of GFP-encoding vectors, transduction was instead analyzed at 44 hpi. Cells were fixed with 4% paraformaldehyde for 15 min, followed by 100% methanol for 15 min at −20 °C, before staining with the hexon monoclonal antibody MAB8052 (Sigma). For detection, an Alexa Fluor 488-conjugated secondary antibody was used. To ensure an intact monolayer, the cells were finally stained with Hoechst 3342 diluted 1:10,000. In all transduction experiments an automatic fluorescent image acquisition was utilized using Trophos Plate RUNNER HD (Dioscure). The images were analyzed using Tina software (Dioscure).

Flow Cytometry Experiments. Cells were detached with PBS-EDTA (phosphate-buffered saline supplemented with 0.05% ethylenediaminetetraacetate), reactivated in CHO cell-growth medium for 1 h at 37 °C, pelleted in 96-well plates (2×10^5 cells per well), and washed once with binding buffer (BB; DMEM supplemented with 20 mM Hepes, 20 U/mL penicillin plus 20 μg/mL streptomycin, and 1% bovine serum albumin; BSA). For detection of CD46, a primary anti-CD46 antibody was added (10 μg/mL in BB) to the cells and incubated for 1 h on ice. Unbound antibodies were washed away with PF buffer (PBS supplemented with 2% FBS), and the cells were then incubated with an Alexa Fluor 488-conjugated secondary antibody (donkey anti-mouse A488; dilution of 1:1,000 in PF; Invitrogen) for 30 min on ice. Thereafter, the cells were washed once with PF and analyzed by flow cytometry using a FACS LSR II instrument (Becton Dickinson).

Transduction Competition Experiments. In fiber knob competition experiments, CHO-CD46 cells were preincubated with 2 μM soluble trimeric fiber knobs at 4 °C for 60 min before virions were added to the cells and incubated for 60 min at 4 °C. Unbound virions and fiber knobs were removed by washing twice with DMEM and the plates were incubated for 24 h at 37 °C in HAMs-F12 media with 2% FBS, 20 mM Hepes, and 1× PenStrep. In experiments where soluble CD46/CAR was used for blocking transduction, CHO-CD46 cells were preincubated with 10 to 250 μg/mL CD46/CAR at 4 °C for 60 min. All subsequent steps were done as described above. In hexon competition experiments, hexons were mixed with wild-type virus in DMEM at room temperature and directly added to the cells. Virus infection was allowed to run for 60 min before the virus/hexon mixture was removed and the cells were washed three times with DMEM and fresh DPH + 2% FBS was added. At 44 hpi, the cells were fixed and stained for hexon production as previously described.

Fiber Knob Cell-Binding Experiments. Binding experiments were performed as described previously (17). Subconfluent cells were detached with PBS-EDTA and recovered in growth medium for 1 h at 37 °C, pelleted in 96-well plates (2×10^5 cells per well), and washed once with binding buffer (DMEM, 1× PenStrep, 20 mM Hepes, 1% BSA). The cells were then incubated with soluble fiber knobs at 10 μg/mL (HAdV-D56, HAdV-B35, and HAdV-B7) in 100 μL binding buffer for 1 h on ice. Unbound fiber knobs were washed away with PFN (PBS containing 2% FBS and 0.01% NaN_3) and the cells were then incubated with an anti–RGS-His mouse monoclonal antibody (Qiagen; diluted 1:200 in PFN) for 30 min. Before the addition of secondary antibody diluted 1:20 in PFN (rabbit anti-mouse fluorescein isothiocyanate antibodies; DakoCytomation), the cells were washed once with PFN. After 30 min on ice, the secondary antibody was removed and the cells were washed with PFN. Bound fiber knob was analyzed by flow cytometry using a FACS LSR II instrument (Becton Dickinson).

Virion Cell-Binding Experiments. Binding assays using ^{35}S-radiolabeled HAdVs were carried out as described previously (17). Briefly, the cells were detached with PBS-EDTA and allowed to recover in growth medium for 1 h. After counting, 2×10^5 cells were added to each well of a 96-well microplate and incubated with 10^4 virions per cell for 60 min on ice. Nonbound virions were then removed by washing using binding buffer (DMEM supplemented with 20 mM Hepes, 1× PenStrep, and 1% FBS) and the cell-associated radioactivity was measured by using a Wallac 1450 MicroBeta counter (TriLux).

Surface Plasmon Resonance Analyses. All measurements between HAdV knobs, HAdV hexons, and HAdV against CD46 were performed at 25 °C using a Biacore T-200 instrument. CD46 was immobilized to a CM5 chip, using the Amine Coupling Kit (GE Healthcare), to a concentration of 4 to 5 ng·mm^2 (~5,000 response units; RUs). All binding assays were performed at 25 °C using running buffer (10 mM Hepes, 150 mM NaCl, 1 mM Ca^{2+}, 1 mM Mg^{2+}, 0.01% [vol/vol] surfactant P20, pH 7.4). The analytes were diluted in running buffer (50 and 25 μg/mL, alternatively only 50 μg/mL), and then injected in series over the reference and experimental biosensor surfaces for 120 s at a flow rate of 30 μL/min. Blank samples containing only running buffer were also injected under the same conditions to allow for double referencing. After each cycle, the biosensor surface was regenerated with a 60-s pulse of 10 mM glycine (pH 1.5) at a flow rate of 30 μL/min.

Fiber Knob Crystallization, Structure Determination, and Homology Modeling. Crystals of the HAdV-D56 fiber knob were grown at 4 °C by sitting drop vapor diffusion over a reservoir of 20% (weight/volume) polyethylene glycol 3350 and 200 mM magnesium nitrate hexahydrate. The crystals were frozen in liquid nitrogen with 20% glycerol as cryoprotectant. Data were collected at beamline X06DA (PXIII) (Swiss Light Source) at a wavelength of 1.0 Å using a Pilatus 2M detector and processed with XDS (55). The structure was solved by molecular replacement with Phaser (56) in CCP4 (57) using a CHAINSAW (58) model derived from the HAdV-D37 fiber knob structure (Protein Data Bank [PDB] ID code 1UXE). Refinement was carried out by manual model building in Coot (59) alternated with restraint refinement including anisotropic B-factor refinement using phenix.refine (60). Coordinates and structure factors have been deposited in the PDB with ID code 7ajp. Figures were prepared using PyMOL (61–63). Data statistics are found in *SI Appendix*, Table S3. Superposition of the fiber knobs and respective complex structure was carried out using the cealign algorithm in PyMOL and the following PDB ID codes: 3exw for HAdV-B7, 3exv for HAdV-B11, and 3o8e for HAdV-B11 in complex with CD46.

Cryo-EM Analysis and Structure Determination of the HAdV-D56–CD46 Complex. Purified HAdV-D56 virions and purified recombinant CD46 (Sino Biological; 12239-H08H) were used at 1.2 and 0.5 mg/mL in PBS (pH 7.4), respectively. Samples were vitrified on Quantifoil Cu R200 2/2 grids (Electron Microscopy Sciences; Q2100CR2). For the HAdV-D56–CD46 complex structure, 60 μL HAdV-D56 was combined with 60 μL CD46 and incubated on ice for 15 min before concentrating to 20 μL using a 30-kDa molecular mass cutoff spin concentrator (Thermo Fisher Scientific; 88504), for a final nominal concentration of 3.6 and 1.5 mg/mL for HAdV-56 and CD46, respectively. Prior to sample application the grids were glow discharged using a Pelco easiGlow device (Ted Pella) at 15 mA for 30 s. Sample was applied by transferring 3 μL of sample onto the grid, which was blotted and plunge frozen in liquid ethane using a Vitrobot plunge freezer (Thermo Fisher Scientific) with the following settings: 22 °C, 80% humidity, blot force −20, and blotting time 3 s. For both conditions, sample was applied twice with a blotting step, using the same settings as above, between applications (64). All data were collected on an FEI Titan Krios transmission electron microscope (Thermo Fisher Scientific) operated at 300 keV and equipped with a Gatan BioQuantum energy filter and a K2 direct electron detector. A condenser 2 aperture of 70 μm and an objective aperture of 100 μm were chosen for data collection. Coma-free alignment was performed with Sherpa (Thermo Fisher Scientific). Data were acquired in parallel illumination mode using EPU (Thermo Fisher Scientific) software at a nominal magnification of 130 kx (1.042-Å object pixel size). One and two datasets were collected for the HAdV-D56 (Fig. 3*C*) and HAdV-D56–CD46 (*SI Appendix*, Fig. S3*D*) structures, respectively. Data collection parameters are listed in *SI Appendix*, Table S4. Data were processed using Relion 3.1 (65). Beam-induced motion was corrected using Relion's MotionCor2 (66) implementation and the per-micrograph contrast transfer function (CTF) was estimated using Gctf (67). Particles were manually picked and subjected to reference-free 2D classification and well-resolved classes were combined and subjected to mask-less three-dimensional (3D) classification, applying icosahedral symmetry [I3 according to Crowther (68)]. A low-pass–filtered (30 Å) volume of HAdV-F41 (69) was used as a reference volume. Particles were classified into two classes, resulting in 93% of particles allocated to one well-resolved class which was used for downstream processing. Three-dimensional refinement was performed using the output of the 3D classification as a reference model, low-pass–filtered to 30 Å, with no additional Fourier padding. The resolution was calculated using the gold standard Fourier shell correlation (FSC) (threshold 0.143) to 4.82 Å (*SI Appendix*, Fig. S3*E*). Figure electron densities were generated using ChimeraX (70). The two datasets of the HAdV-D56–CD46 complex were processed separately, as for the HAdV-D56 structure, up until and including reference-free 2D classification and merged subsequently for 3D classification. The resolution for the final reconstruction was calculated using the gold standard FSC (threshold 0.143) to 5.11 Å (*SI Appendix*, Fig. S3*F*). Figure electron densities were generated using ChimeraX (70). A difference map $\Delta\rho$ between the virus–receptor complex HAdV-D56–CD46 and the apo virus HAdV-D56 was calculated using EMAN2 (71).

Species D Adenovirus Competition Infection Experiments. A549 cells (20,000) were seeded in a black 96-well plate and 24 h post seeding infected with $CsCl_2$-purified HAdV-C5 or D13/17/23/24/25/26/28/32/37/38/39/42/43/45/46/48/56. Each virus was titrated in order to produce an even amount (ca 10%) of infected cells. After one round of titration, the experiment was set up with or without CD46 present (50 μg/mL). After 60 min, virus unable to infect was removed and the cells were washed once with DMEM. After 44 h the cells were fixed and stained for hexon production using MAB8052 as previously described.

Homology Alignment and Phylogenetic Tree Analyses. Full-length hexon sequences from all HAdV-D types (2) were used for amino acid sequence alignment and phylogenetic tree construction (neighbor-joining tree without distance corrections) using CLUSTAL Omega (72) and TreeDyn for visualization (73). Fiber knob amino acid sequences were aligned starting from the TLWT motif with CLUSTAL Omega.

Statistics. All experiments were performed at least three times with duplicate or triplicate samples in each experiment. The results are expressed as means ± SEM, and two-way ANOVA was performed using GraphPad Prism, version 7.00 for Windows. P values of <0.05 were considered statistically significant.

Data Availability. The X-ray structural data reported in this article have been deposited in the Protein Data Bank with ID code 7AJP.

ACKNOWLEDGMENTS. Cryo-EM data were collected at the Umeå Core Facility for Electron Microscopy (SciLifeLab National Cryo-EM Facility and part of National Microscopy Infrastructure; NMI VR-RFI 2016-00968). We gratefully acknowledge the Swiss Light Source (Villigen, Switzerland) for beam time and the staff at beamline X06DA for assistance during data collection. Funding: Seventh Framework Programme; Marie-Curie Actions (324325 AD-VEC) (to N.A.), Human Frontier Science Program (CDA00047/2017-C) and Knut och Alice Wallenbergs Stiftelse (Wallenberg Centre for Molecular Medicine Fellowship) (to L.-A.C.), Stiftelsen Olle Engkvist Byggmästare (postdoctoral fellowship) (to K.R.), and Baden-Wurttemberg Foundation (M.S.).

1. W. S. M. Wold, M. G. Ison, "Adenoviruses" in *Fields Virology*, D. M. Knipe, P. M. Howley, Eds. (Wolters Kluwer, Philadelphia, ed. 6, 2013), vol. 2, pp. 1732–1767.
2. Human Adenovirus Working Group, Adenovirus classification. http://hadvwg.gmu.edu/. Accessed 1 July 2019.
3. Z. T. Camacho, M. A. Turner, M. A. Barry, E. A. Weaver, CD46-mediated transduction of a species D adenovirus vaccine improves mucosal vaccine efficacy. *Hum. Gene Ther.* **25**, 364–374 (2014).
4. P. Penaloza-MacMaster *et al.*, Alternative serotype adenovirus vaccine vectors elicit memory T cells with enhanced anamnestic capacity compared to Ad5 vectors. *J. Virol.* **87**, 1373–1384 (2013).
5. H. Li *et al.*, Adenovirus serotype 26 utilizes CD46 as a primary cellular receptor and only transiently activates T lymphocytes following vaccination of rhesus monkeys. *J. Virol.* **86**, 10862–10865 (2012).
6. J. E. Teigler, M. J. Iampietro, D. H. Barouch, Vaccination with adenovirus serotypes 35, 26, and 48 elicits higher levels of innate cytokine responses than adenovirus serotype 5 in rhesus monkeys. *J. Virol.* **86**, 9590–9598 (2012).
7. D. H. Barouch *et al.*, International seroepidemiology of adenovirus serotypes 5, 26, 35, and 48 in pediatric and adult populations. *Vaccine* **29**, 5203–5209 (2011).

8. N. B. Mercado *et al*., Single-shot Ad26 vaccine protects against SARS-CoV-2 in rhesus macaques. *Nature* **586**, 583–588 (2020).
9. D. Y. Logunov *et al*., Safety and immunogenicity of an rAd26 and rAd5 vector-based heterologous prime-boost COVID-19 vaccine in two formulations: Two open, non-randomised phase 1/2 studies from Russia. *Lancet* **396**, 887–897 (2020).
10. L. H. Tostanoski *et al*., Ad26 vaccine protects against SARS-CoV-2 severe clinical disease in hamsters. *Nat. Med.* **26**, 1694–1700 (2020).
11. D. H. Barouch *et al*., Evaluation of a mosaic HIV-1 vaccine in a multicentre, randomised, double-blind, placebo-controlled, phase 1/2a clinical trial (APPROACH) and in rhesus monkeys (NHP 13-19). *Lancet* **392**, 232–243 (2018).
12. K. Williams *et al*., Phase 1 safety and immunogenicity study of a respiratory syncytial virus vaccine with an adenovirus 26 vector encoding prefusion F (Ad26.RSV.preF) in adults aged ≥60 years. *J. Infect. Dis.* **222**, 979–988 (2020).
13. I. D. Milligan *et al*., Safety and immunogenicity of novel adenovirus type 26- and modified vaccinia Ankara-vectored Ebola vaccines: A randomized clinical trial. *JAMA* **315**, 1610–1623 (2016).
14. R. A. Larocca *et al*., Adenovirus vector-based vaccines confer maternal-fetal protection against Zika virus challenge in pregnant IFN-$\alpha\beta R^{-/-}$ mice. *Cell Host Microbe* **26**, 591–600.e4 (2019).
15. J. M. Bergelson *et al*., Isolation of a common receptor for Coxsackie B viruses and adenoviruses 2 and 5. *Science* **275**, 1320–1323 (1997).
16. P. W. Roelvink *et al*., The coxsackievirus-adenovirus receptor protein can function as a cellular attachment protein for adenovirus serotypes from subgroups A, C, D, E, and F. *J. Virol.* **72**, 7909–7915 (1998).
17. A. Lenman *et al*., Human adenovirus 52 uses sialic acid-containing glycoproteins and the coxsackie and adenovirus receptor for binding to target cells. *PLoS Pathog.* **11**, e1004657 (2015).
18. A. Segerman *et al*., Adenovirus type 11 uses CD46 as a cellular receptor. *J. Virol.* **77**, 9183–9191 (2003).
19. A. Gaggar, D. M. Shayakhmetov, A. Lieber, CD46 is a cellular receptor for group B adenoviruses. *Nat. Med.* **9**, 1408–1412 (2003).
20. H. Wang *et al*., Desmoglein 2 is a receptor for adenovirus serotypes 3, 7, 11 and 14. *Nat. Med.* **17**, 96–104 (2011).
21. E. Vassal-Stermann *et al*., CryoEM structure of adenovirus type 3 fibre with desmoglein 2 shows an unusual mode of receptor engagement. *Nat. Commun.* **10**, 1181 (2019).
22. A. T. Baker, R. M. Mundy, J. A. Davies, P. J. Rizkallah, A. L. Parker, Human adenovirus type 26 uses sialic acid-bearing glycans as a primary cell entry receptor. *Sci. Adv.* **5**, eaax3567 (2019).
23. E. C. Nilsson *et al*., The GD1a glycan is a cellular receptor for adenoviruses causing epidemic keratoconjunctivitis. *Nat. Med.* **17**, 105–109 (2011).
24. J. Liu *et al*., Human adenovirus type 17 from species D transduces endothelial cells and human CD46 is involved in cell entry. *Sci. Rep.* **8**, 13442 (2018).
25. N. Belousova *et al*., Native and engineered tropism of vectors derived from a rare species D adenovirus serotype 43. *Oncotarget* **7**, 53414–53429 (2016).
26. A. A. C. Lemckert *et al*., Generation of a novel replication-incompetent adenoviral vector derived from human adenovirus type 49: Manufacture on PER.C6 cells, tropism and immunogenicity. *J. Gen. Virol.* **87**, 2891–2899 (2006).
27. E. Wu *et al*., Membrane cofactor protein is a receptor for adenoviruses associated with epidemic keratoconjunctivitis. *J. Virol.* **78**, 3897–3905 (2004).
28. P. Abbink *et al*., Comparative seroprevalence and immunogenicity of six rare serotype recombinant adenovirus vaccine vectors from subgroups B and D. *J. Virol.* **81**, 4654–4663 (2007).
29. C. A. Kahl *et al*., Potent immune responses and in vitro pro-inflammatory cytokine suppression by a novel adenovirus vaccine vector based on rare human serotype 28. *Vaccine* **28**, 5691–5702 (2010).
30. S. Lecollinet *et al*., Improved gene delivery to intestinal mucosa by adenoviral vectors bearing subgroup B and D fibers. *J. Virol.* **80**, 2747–2759 (2006).
31. S. A. Trauger, E. Wu, S. J. Bark, G. R. Nemerow, G. Siuzdak, The identification of an adenovirus receptor by using affinity capture and mass spectrometry. *ChemBioChem* **5**, 1095–1099 (2004).
32. B. D. Persson *et al*., Adenovirus type 11 binding alters the conformation of its receptor CD46. *Nat. Struct. Mol. Biol.* **14**, 164–166 (2007).
33. L. Lasswitz, N. Chandra, N. Arnberg, G. Gerold, Glycomics and proteomics approaches to investigate early adenovirus-host cell interactions. *J. Mol. Biol.* **430**, 1863–1882 (2018).
34. M. R. Duffy *et al*., Generation and characterization of a novel candidate gene therapy and vaccination vector based on human species D adenovirus type 56. *J. Gen. Virol.* **99**, 135–147 (2018).
35. H. V. Trinh *et al*., Avidity binding of human adenovirus serotypes 3 and 7 to the membrane cofactor CD46 triggers infection. *J. Virol.* **86**, 1623–1637 (2012).
36. L. Pache, S. Venkataraman, V. S. Reddy, G. R. Nemerow, Structural variations in species B adenovirus fibers impact CD46 association. *J. Virol.* **82**, 7923–7931 (2008).
37. A. Gaggar, D. M. Shayakhmetov, M. K. Liszewski, J. P. Atkinson, A. Lieber, Localization of regions in CD46 that interact with adenovirus. *J. Virol.* **79**, 7503–7513 (2005).
38. C. Fleischli *et al*., Species B adenovirus serotypes 3, 7, 11 and 35 share similar binding sites on the membrane cofactor protein CD46 receptor. *J. Gen. Virol.* **88**, 2925–2934 (2007).
39. B. D. Persson *et al*., An arginine switch in the species B adenovirus knob determines high-affinity engagement of cellular receptor CD46. *J. Virol.* **83**, 673–686 (2009).
40. S. N. Waddington *et al*., Adenovirus serotype 5 hexon mediates liver gene transfer. *Cell* **132**, 397–409 (2008).
41. L. H. Stockwin *et al*., Engineered expression of the Coxsackie B and adenovirus receptor (CAR) in human dendritic cells enhances recombinant adenovirus-mediated gene transfer. *J. Immunol. Methods* **259**, 205–215 (2002).
42. L. M. Ebert *et al*., A non-canonical role for desmoglein-2 in endothelial cells: Implications for neoangiogenesis. *Angiogenesis* **19**, 463–486 (2016).
43. F. C. Zhu *et al*., Immunogenicity and safety of a recombinant adenovirus type-5-vectored COVID-19 vaccine in healthy adults aged 18 years or older: A randomised, double-blind, placebo-controlled, phase 2 trial. *Lancet* **396**, 479–488 (2020).
44. T. C. Mast *et al*., International epidemiology of human pre-existing adenovirus (Ad) type-5, type-6, type-26 and type-36 neutralizing antibodies: Correlates of high Ad5 titers and implications for potential HIV vaccine trials. *Vaccine* **28**, 950–957 (2010).
45. N. Chandra *et al*., Sialic acid-containing glycans as cellular receptors for ocular human adenoviruses: Implications for tropism and treatment. *Viruses* **11**, E395 (2019).
46. I. Kirby *et al*., Adenovirus type 9 fiber knob binds to the coxsackie B virus-adenovirus receptor (CAR) with lower affinity than fiber knobs of other CAR-binding adenovirus serotypes. *J. Virol.* **75**, 7210–7214 (2001).
47. E. Seiradake, H. Lortat-Jacob, O. Billet, E. J. Kremer, S. Cusack, Structural and mutational analysis of human Ad37 and canine adenovirus 2 fiber heads in complex with the D1 domain of coxsackie and adenovirus receptor. *J. Biol. Chem.* **281**, 33704–33716 (2006).
48. C. Y. Chiu *et al*., Structural analysis of a fiber-pseudotyped adenovirus with ocular tropism suggests differential modes of cell receptor interactions. *J. Virol.* **75**, 5375–5380 (2001).
49. R. W. Walters *et al*., Adenovirus fiber disrupts CAR-mediated intercellular adhesion allowing virus escape. *Cell* **110**, 789–799 (2002).
50. J. Rebetz *et al*., Fiber mediated receptor masking in non-infected bystander cells restricts adenovirus cell killing effect but promotes adenovirus host co-existence. *PLoS One* **4**, e8484 (2009).
51. M. K. Liszewski, J. P. Atkinson, Membrane cofactor protein (MCP; CD46). Isoforms differ in protection against the classical pathway of complement. *J. Immunol.* **156**, 4415–4421 (1996).
52. C. Johansson *et al*., Adenoviruses use lactoferrin as a bridge for CAR-independent binding to and infection of epithelial cells. *J. Virol.* **81**, 954–963 (2007).
53. J. M. Casasnovas, M. Larvie, T. Stehle, Crystal structure of two CD46 domains reveals an extended measles virus-binding surface. *EMBO J.* **18**, 2911–2922 (1999).
54. M. C. Bewley, K. Springer, Y. B. Zhang, P. Freimuth, J. M. Flanagan, Structural analysis of the mechanism of adenovirus binding to its human cellular receptor, CAR. *Science* **286**, 1579–1583 (1999).
55. W. Kabsch, XDS. *Acta Crystallogr. D Biol. Crystallogr.* **66**, 125–132 (2010).
56. A. J. McCoy *et al*., Phaser crystallographic software. *J. Appl. Crystallogr.* **40**, 658–674 (2007).
57. M. D. Winn *et al*., Overview of the CCP4 suite and current developments. *Acta Crystallogr. D Biol. Crystallogr.* **67**, 235–242 (2011).
58. K. Hata *et al*., Limited inhibitory effects of oseltamivir and zanamivir on human sialidases. *Antimicrob. Agents Chemother.* **52**, 3484–3491 (2008).
59. P. Emsley, B. Lohkamp, W. G. Scott, K. Cowtan, Features and development of Coot. *Acta Crystallogr. D Biol. Crystallogr.* **66**, 486–501 (2010).
60. P. V. Afonine *et al*., Towards automated crystallographic structure refinement with phenix.refine. *Acta Crystallogr. D Biol. Crystallogr.* **68**, 352–367 (2012).
61. The PyMOL Molecular Graphics System (Version 1.8, Schrödinger, LLC, 2015).
62. N. A. Baker, D. Sept, S. Joseph, M. J. Holst, J. A. McCammon, Electrostatics of nanosystems: Application to microtubules and the ribosome. *Proc. Natl. Acad. Sci. U.S.A.* **98**, 10037–10041 (2001).
63. T. J. Dolinsky *et al*., PDB2PQR: Expanding and upgrading automated preparation of biomolecular structures for molecular simulations. *Nucleic Acids Res.* **35**, W522–W525 (2007).
64. J. Snijder *et al*., Vitrification after multiple rounds of sample application and blotting improves particle density on cryo-electron microscopy grids. *J. Struct. Biol.* **198**, 38–42 (2017).
65. J. Zivanov, T. Nakane, S. H. W. Scheres, Estimation of high-order aberrations and anisotropic magnification from cryo-EM data sets in *RELION*-3.1. *IUCrJ* **7**, 253–267 (2020).
66. J. Bergqvist *et al*., Detection and isolation of Sindbis virus from mosquitoes captured during an outbreak in Sweden, 2013. *Vector Borne Zoonotic Dis.* **15**, 133–140 (2015).
67. K. Zhang, Gctf: Real-time CTF determination and correction. *J. Struct. Biol.* **193**, 1–12 (2016).
68. R. A. Crowther, Procedures for three-dimensional reconstruction of spherical viruses by Fourier synthesis from electron micrographs. *Philos. Trans. R. Soc. Lond. B Biol. Sci.* **261**, 221–230 (1971).
69. K. Rafie, The structure of enteric human adenovirus 41—A leading cause of diarrhea in children. *Sci. Adv.* In press.
70. T. D. Goddard *et al*., UCSF ChimeraX: Meeting modern challenges in visualization and analysis. *Protein Sci.* **27**, 14–25 (2018).
71. G. Tang *et al*., EMAN2: An extensible image processing suite for electron microscopy. *J. Struct. Biol.* **157**, 38–46 (2007).
72. F. Madeira *et al*., The EMBL-EBI search and sequence analysis tools APIs in 2019. *Nucleic Acids Res.* **47**, W636–W641 (2019).
73. F. Chevenet, C. Brun, A. L. Bañuls, B. Jacq, R. Christen, TreeDyn: Towards dynamic graphics and annotations for analyses of trees. *BMC Bioinformatics* **7**, 439 (2006).